Journal of Applied Sciences

ISSN 1812-5654

science alert

ANSInet
an open access publisher
http://ansinet.com

Journal of Applied Sciences 14 (6): 518-524, 2014
ISSN 1812-5654 / DOI: 10.3923/jas.2014.518.524

Wind Characteristics Around a Long-span Bridge in Mountainous Terrain

[1,2]Chunping Tang, [1]Liangliang Zhang, [1]Jingyun Hang and [1]Haiyang Zhang
[1]College of Civil Engineering, Chongqing University, 400045, Chongqing, China
[2]Chongqing Technology and Business Institute, 400052, Chongqing, China

Abstract: The study aims at investigating the aeolian turbulent environment around a long-span bridge site in mountainous terrain in western China. Anemometers were installed over the height of the bridge site to measure both instantaneous wind speed and direction as well as their means. Turbulence intensity results showed that, the mean wind speed at the site presented complex variations over its height,the turbulence intensity at height of 10 m above the arch springing exceeded 40% and at 90 m it was still as high as 15%. The site's wind speed profile did not follow either logarithmic or exponential models. The measured horizontal turbulent wind speed spectrum was closer to an Irwin spectrum, but differed from the Simiu spectrum: vertical turbulent wind speed spectra differed from the Panofsky spectrum.

Key words: Bridges, wind, mountainous terrain, field observation, turbulence, power spectrum

INTRODUCTION

With more bridge construction projects taking place in mountainous areas in recent years, the structural engineer faces a difficulty, namely, the characterisation of the wind environment in mountainous terrain (Zhang *et al*., 2008, 2010). Most of the wind characteristics of plains and coastal areas are analysed according to Class A or B landforms. Corresponding parameters for the mean wind profile and turbulence characteristics of these two landforms are given in China's "Wind-resistant design specification for highway bridges" (Professional Standard PRC, 2004) (referred to henceforth as the Specification). These parameters can be directly applied in wind-resistance calculations and wind tunnel tests. However, mountainous areas present landform and terrain variations and complex wind-field distributions. The current Specification is only suitable for an isotropic wind-field over a flat landform. However, the wind characteristics of mountainous areas, with their complex terrains and landforms, differ greatly from those in the Specification. Thus it is necessary to modify these parameters using field measurements and wind tunnel tests while especially investigating a bridge's wind-resistance under a mountainous terrain's wind characteristics.

In wind engineering, wind speed is usually considered as comprising two components: the turbulence that generates gusts or calm winds and the mean wind speed. Of these components, turbulence exhibits intensive non-linear random fluctuations in both space and time (Simiu and Scanlan, 1996; Sharma and Richards, 1999). To study the wind-resistance of a large span bridge, it is firstly required to more accurately simulate and define the wind characteristics around the bridge site. Therefore, measurement and statistical analysis were used as the main approaches to this study (Xian *et al*., 2008; Gang, 2012; Zhang *et al*., 2006). This study concerned a long-span bridge in the mountainous area of western China as Fig. 1 shows. Anemometers were installed up the height of the construction tower on the bridge site. Using the anemometers, the wind environment characteristics around the bridge site were measured. Site parameters such as: Wind speed, turbulence intensity, turbulent wind power spectrum density function, turbulence integral scale, etc., were then analysed.

MEASUREMENT METHODS OF THE WIND CHARACTERISTICS

Measurement instruments: A PH anemometer was used to measure wind characteristics over the range zero to 60 m sec^{-1} at a precision of <3 mm sec^{-1}. Data-logging through a computer's serial port allowed for the acquisition and real-time storage of high frequency data and uninterrupted wind speed observations. To obtain the distribution characteristics of wind turbulence at the bridge site and meet the wind field requirements for bridge wind-resistance design (Andersen and Lovseth, 1995), nine PH anemometers were installed. They were installed towards the north up the height of the bridge site (one per 10 m) as Fig. 2 shows. Using these anemometers, the direction and speed of instantaneous wind and mean wind were measured. Wind direction was defined by compass bearing (i.e., a northerly blew from 0°).

Corresponding Author: Chunping Tang, College of Civil Engineering, Chongqing University, 400045, Chongqing, China

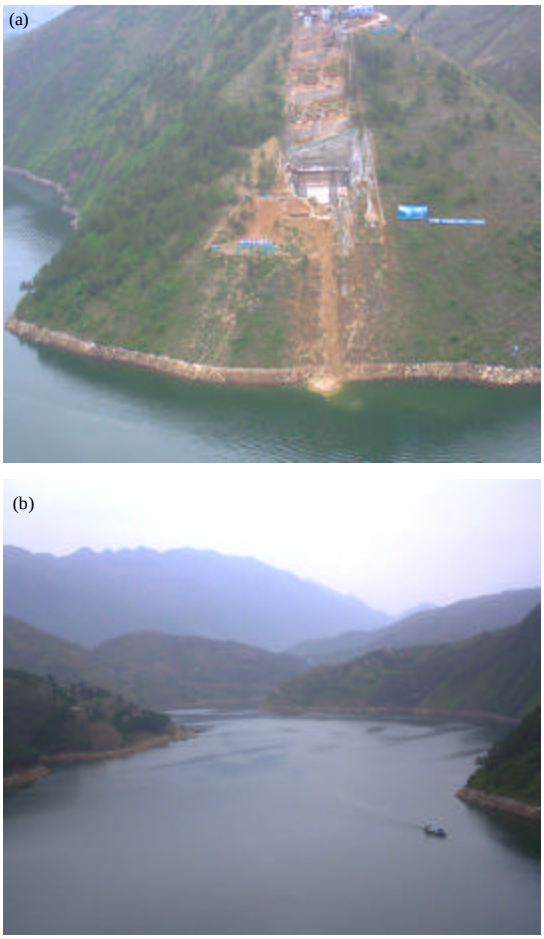

Fig. 1(a-b): Study site for, (a, b) Long-span bridge in the mountainous area

Fig. 2: Anemometer installed at 90 m above the arch springing

Principles behind wind turbulence: Studies of the wind characteristics often assume a neutral boundary layer and do not consider the influence of the temperature gradient. Generally (Pasquill, 1974), neutral boundary layers are observed during strong wind weather events with mean wind speeds above 6 m sec^{-1}. Meanwhile, the study of bridge wind-resistance mainly considers the effect of turbulent wind. In meteorology, wind above scale 5 is classified as gale force. According to the Beaufort wind scale, the lower limit of a scale 5 wind is 8 m sec^{-1}. Only wind at, or above, a certain scale can induce excessive load or vibration to an extent affecting the safety of a bridge structure (Gu *et al*., 2002; Ai and Xing, 2012; Ge *et al*., 2002; Lin *et al*., 2008; Shum *et al*., 2008). Typically, in addition to the vortex-induced vibrations of a flexible large-span bridge are caused by wind speeds of approximately 8 m sec^{-1} while other vibrations (including flutter, buffeting and galloping) are caused by wind speeds above 8 m sec^{-1}. Comprehensive analysis showed that the low limit of 10 min mean speed of the wind's turbulence in this study was 8.0 m sec^{-1}.

Data processing method: Before processing the measurements, original data were pre-treated. Invalid data (those influenced by rainfall, environment and the stability of data acquisition system) were removed: Only valid data exceeding 90% reliability were involved in subsequent calculations.

Turbulence characteristic analysis was based on 10 min intervals. Ten-minute sub-samples were divided according to date and time sequence. Then those valid rates of the sub-samples were re-calculated. Only sub-samples with a valid rate of more than 95% could be used in the analysis of turbulence characteristics. Moreover, in the analysis of integral scale and frequency spectrum, the invalid data points which were deleted should be completed by incorporation at corresponding times and positions. The integrity of time information and consistency of sample length, were thereby ensured.

In wind engineering, the structural scale is smaller than the meteorological scale. The study of wind characteristics mainly concentrates on the wind characteristics of nearby regions and mainly includes. The mean wind speed and direction, turbulence intensity, gust factor, turbulence integral scale and turbulent wind speed power spectrum.

Mean wind speed and direction: It is assumed that the 3-D wind sequence measured by an anemometer is $u_x(t)$, $u_y(t)$ and $u_z(t)$. Using a vector decomposition method, the horizontal mean wind speed U and wind direction angle ϕ in any 10 min interval can be obtained thus:

$$U = \sqrt{\overline{u_x(t)}^2 + \overline{u_y(t)}^2} \quad (1)$$

$$\cos\phi = \frac{\overline{u_x(t)}}{U} \quad (2)$$

Since the vertical wind speed direction aligns with the *z*-axis in anemometer coordinates, the vertical mean wind speed is obtained from Eq. 3:

$$W = \overline{u_z(t)} \quad (3)$$

where, $\overline{u_x(t)}$, $\overline{u_y(t)}$ and $\overline{u_z(t)}$ are the 3-D mean wind speeds of the sample in a 10 min interval. Based on the calculation of the mean wind speed above, the formulae for longitudinal turbulent wind speed u_t, transverse turbulent wind speed v_t and vertical turbulent wind speed w_t can be obtained thus:

$$u_t = u_x(t)\cos\phi + u_y(t)\sin\phi - U \quad (4)$$

$$v_t = u_x(t)\sin\phi + u_y(t)\cos\phi - U \quad (5)$$

$$w_t = u_z(t) - W \quad (6)$$

Turbulence intensity: Turbulence intensity reflects the fluctuating intensity of wind. It is the simplest parameter used to describe atmospheric turbulence. According to the Specification, turbulence intensity is defined as the ratio of the mean square root of the turbulent wind speed and the horizontal mean wind speed in a 10 min interval. Turbulence intensities of longitudinal turbulence speed u(t), transverse turbulent wind speed v(t) and vertical turbulent wind speed w(t) can be expressed by Eq. 7-9:

$$I_u(z) = \frac{\sigma_u}{U(z)} \quad (7)$$

$$I_v(z) = \frac{\sigma_v}{U(z)} \quad (8)$$

$$I_w(z) = \frac{\sigma_w}{U(z)} \quad (9)$$

where, σ_u, σ_v, σ_w are the mean square roots of the turbulent wind speed u(t), v(t) and w(t) respectively; U(z) is the mean wind speed at height z above ground.

Gust factor: The turbulence intensity of wind can also be represented by its gust factor $G(t_g)$, defined as the ratio of the maximum mean wind speed in gust duration time t_g (usually, the gust duration in structural wind engineering is 2-3 sec: t_g was chosen as 3 sec for this study) to the mean wind speed during a basic time interval (Xie *et al*., 2009), namely:

$$G_u(t_g) = 1 + \frac{\max[\bar{u}(t_g)]}{U(z)} \quad (10)$$

$$G_v(t_g) = \frac{\max[\bar{v}(t_g)]}{U(z)} \quad (11)$$

where, $\bar{u}(t_g)$, $\bar{v}(t_g)$ are the mean values of the along-wind and cross-wind turbulent wind speed in time t_g respectively.

Turbulence integral scale: The mathematical expression of turbulence integral scale is:

$$L_u^x = \frac{1}{\sigma_u^2}\int_0^\infty R_{12}(x)dx \quad (12)$$

In Eq. 12, $R_{12}(x)$ is the correlation function of two longitudinal turbulent wind speeds ($u_1(x_1, y_1, z_1, t)$ and $u_2(x_1+x, y_1, z_1, t)$; t is the time; σ_u is the variance of turbulence speed u and $R(0) = \sigma_u^2$. Assuming that a turbulent vortex migrates at speed U(z), turbulence speed U(z) can be defined by $u(x-x'/U(z), \tau)$. The integral scale of turbulence can be calculated using the autocorrelation function in Eq. 13:

$$R(\tau) = \frac{\lim_{T\to\infty}\frac{1}{T}\int_0^T u(x,t)u(x,t+\tau)d\tau}{\sigma_u^2(x)} \quad (13)$$

Turbulence power spectrum density function: The turbulent wind speed power spectra in different countries' specifications differ. The horizontal turbulent wind speed spectrum in the wind-resistant design currently used in China is as follows:

$$\frac{nS_u(z,n)}{u_*^2} = \frac{200f}{(1+50f)^{5/3}} \quad (14)$$

The vertical turbulent wind speed spectrum usually follows Eq. 15:

$$\frac{nS_w(z,n)}{u_*^2} = \frac{6f}{(1+4f)^2} \quad (15)$$

where, $f = nz/U$, z is the height from the ground, u_* is the friction speed, $u_*^2 = \sigma_u^2/\beta$ and β is the friction speed coefficient.

ANALYSIS OF MEASUREMENT RESULTS

Mean wind speed and direction: Figure 3 present the wind-roses during winter and summer: winter mainly saw northeast winds while summer saw prevailing southeast and south winds.

Figure 4 shows the wind speed time history curve measured by sensors at a height of 70 m above the arch springing during certain periods of summer and winter. Since the measurement was only conducted for slightly more than one year, it would be less reliable to calculate the basic 1 in 100 year wind speed for this site using the data obtained. Considering this situation, the cross threshold method (peak over threshold method) that only needed a small number of samples was used in subsequent calculations. Using this method, the weight of the maximum wind speed was reduced. Meanwhile, most of the maximum wind speeds in one year were retained. Thus it became possible to estimate extreme wind speeds using shorter wind speed sequences: The basic wind speed was calculated thus:

$$V_{max} = v_g\text{-}b\{1\text{-}[\mu_0 n(v_s)T/N]^c\}/c \qquad (16)$$

where, v_s is the wind speed threshold, b and c are scale and shape parameters respectively, μ_0 is the annual average incidence of a given wind speed, $n(v_s)$ is the average occurrence times of extreme wind speed (the wind speed exceeds threshold v_s) and N is the annual average number of times the wind speed exceeded a certain value. Using Eq. 16 the basic 1 in 100 year wind speed for this site was calculated as 26.8 m sec^{-1}.

Turbulence intensity: Figure 5 show the variations in turbulence intensity at 10 and 90 m, above the arch springing respectively. In both Figure 5a and b, the turbulence intensity at 10 m above the arch springing exceeded 40%, with individual points exceeding 50%; the turbulent intensity at 90 m was above 15%. The results implied that, in typically mountainous areas, the turbulence intensity was far greater than recommended values in the Specification. Turbulent wind posed serious problems and would be a prime cause of bridge buffeting.

Gust factor: According to the measured data, the ratio of the maximum mean wind speed and horizontal mean wind speed in the gust duration time t_g measured by sensors at different heights was calculated. Using this ratio, the gust factors in cross- and along-wind directions were obtained. Then the gust factors were weighted and averaged to acquire the gust factor value for each day. Finally, the variation laws of the gust factors at different heights were

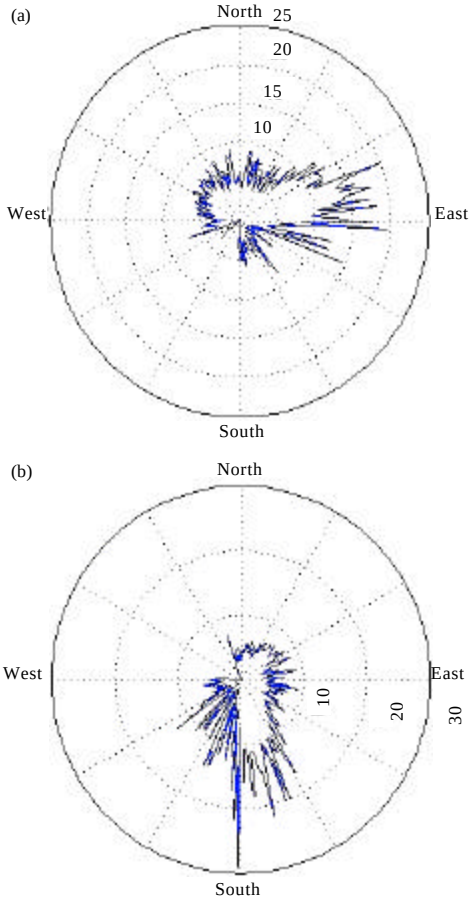

Fig. 3(a-b): Wind-rose (m sec^{-1}), (a) Winter and (b) Summer

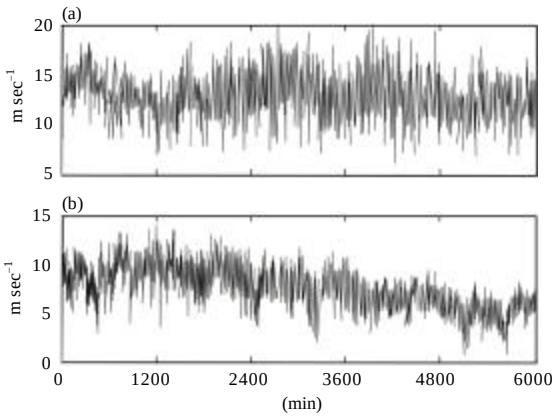

Fig. 4(a-b): (a) Field observation data of wind-speed at the bridge site (summer) and (b) Field observation data of wind-speed at the bridge site (winter)

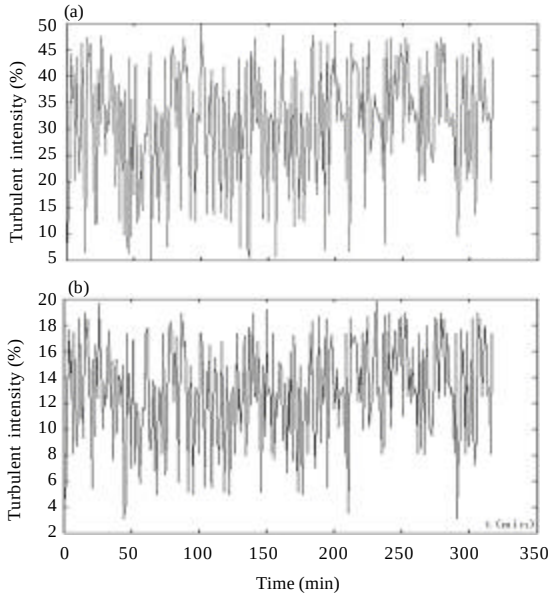

Fig. 5(a-b): (a) Turbulence intensity at 10 m above the arch springing and (b) Turbulence intensity at 90 m above the arch springing

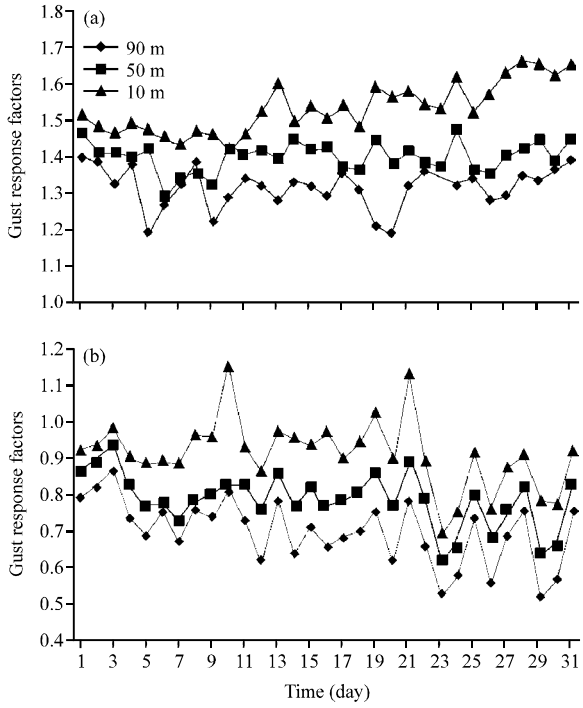

Fig. 6(a-b): (a) Time-history curve of the gust factor: Along-wind direction and (b) Time-history curve of the gust factor: Cross-wind direction

derived, that is, the gust factor's time-history curves were obtained. For brevity's sake, only the January time-history curves for the gust factor at heights: 10, 50 and 90 m above the arch springing are shown as Fig. 6a and b.

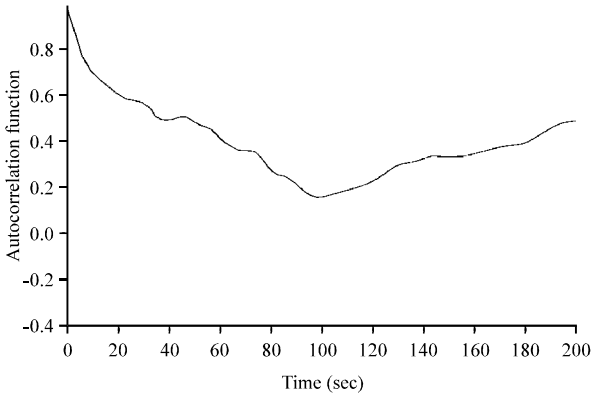

Fig. 7: Autocorrelation function: Turbulent wind speed, 10 m above the arch springing

For mountainous terrain, in the along-wind direction, the maximum value of the gust factor at 10 m above the arch springing was observed in August, with a value about 1.6 while that at 90 m occurred in January, with a value of about 1.4; in the cross-wind direction, the maximum value of the gust factor at 10 m above the arch springing was observed in January, with a value about 1.15 while that at 90 m above the arch springing occurred in January and March, with a value of around 0.8. On the whole, the down-wind turbulence intensity in mountainous terrain was higher than that on the plains. Turbulent winds can easily cause buffeting of bridge structures.

Turbulence integral scale: Figure 7 shows the autocorrelation function of the turbulent wind speed at a height of 10 m above the arch springing: Only when $\tau \to \infty$, did the autocorrelation function $R(\tau)$ tend to zero. To obtain accurate T_u values, the sampling time should be extended towards infinity. Therefore, as this was impossible, the turbulence integral scale L^x_u obtained by autocorrelation function $R(\tau)$ was prone to error and a new analysis method was needed.

Therefore, a "spectrum fitting" technique was used to obtain turbulence integral scale. The wind speed spectrum curve in Fig. 7 was compared to the von-Karman spectrum and the formula $L^x_u = T_u U(z)$, respectively. When regularisation coordinates were used, the spectrum shape in Fig. 7 was basically the same as the von Karman spectrum's shape. The wind speed spectrum, as expressed by von-Karman spectrum and $L^x_u = T_u U(z)$, provided the relationship between wind speed spectrum and turbulence integral scale. Therefore, through iterative fitting of the relationship formula, corresponding

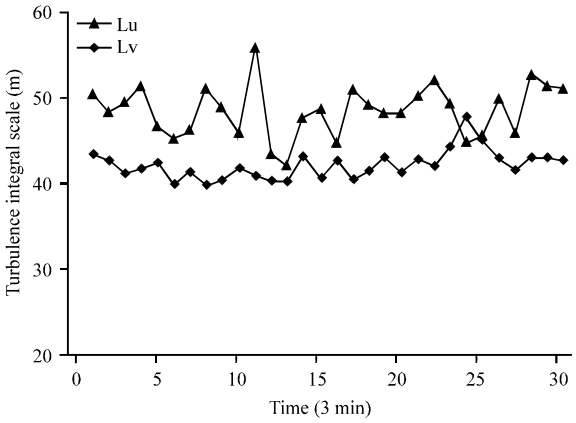

Fig. 8: Turbulence integral scale

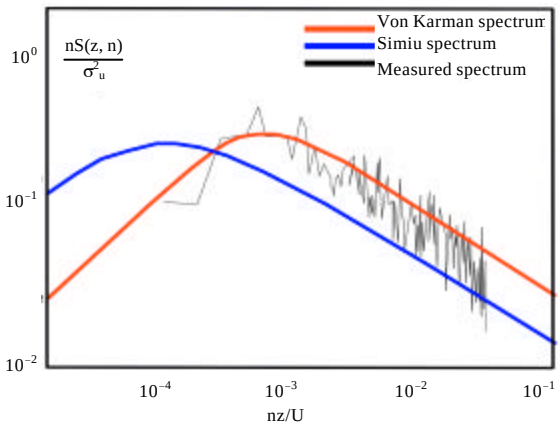

Fig. 9: Vertical turbulent wind speed power spectrum curve

turbulence integral scales could be obtained. The comparison of the turbulence integral scales obtained by spectrum fitting method and autocorrelation function indicated that, with increased sampling time, the results of the two methods became closer.

The turbulence integral scale obtained by analysing the measured data is shown in Fig. 8: The mean value of the turbulence integral scale in the along-wind direction was 48.5 m while that in the cross-wind direction was 42.1 m. These two values were only about 70% of the standard values.

Turbulence power spectrum: To investigate the relationship governing the variations in the turbulence power spectrum, the horizontal and vertical turbulent power spectrums of the wind speed at a height of 10 m above the arch springing were drawn using log-log coordinates, as shown in Fig. 9 where frequency nz/U forms the abscissa and $nS(z, n)/\sigma_u^2$ the ordinate. For

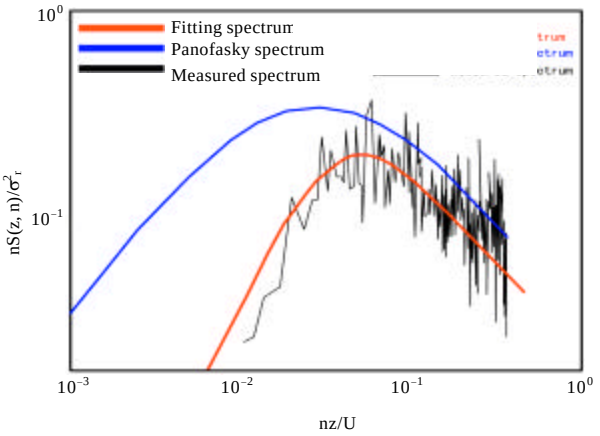

Fig. 10: Vertical turbulent wind speed power spectrum

convenience when comparing, Fig. 9 also displays the von Karman and Simiu, spectra from the Specification.

Figure 10 shows the vertical turbulent wind power spectrum curve at a height of 10 m. For convenience when comparing, Fig. 10 also shows the simulated spectrum represented by Eq. 17 and the Panofsky spectrum from the Specification.

In Fig. 9 and 10, the measured horizontal turbulent wind speed spectrum was relatively close to the von-Karman spectrum, but showed greater differences from the Simiu spectrum; the peak values of the wind speed power spectrum curve shifted towards the higher frequency band; the vertical wind spectrum curve presented larger differences between it and the Panofsky spectrum recommend in the Specification. The relationship between them was fitted using (17), i.e.,:

Vertical turbulent wind speed spectrum:

$$\frac{nS_w(z,n)}{\sigma_w^2} = \frac{5.15(nL_w^x / U(z))}{[1+4.77\frac{nL_w^x}{U(z)}]^2} \quad (17)$$

Test results for one year showed that, due to the larger fluctuations caused by mountainous terrain, the concept of basic wind speed in the Specification was not applicable to this site and its innate complexities; the average wind speed showed complicated variations with height and the wind profile did not fit either logarithmic, or exponential, models commonly used.

The turbulence intensity and gust factor of western mountainous areas were significantly greater than the reference values in the Specification while the turbulence integral scale was much smaller than that recommended by the Specification. The peaks of turbulent wind speed power spectrum shifted to the higher frequency band.

The power spectral model of the turbulent wind speed was possibly able to be simulated using Eq. 18 and 19.

Horizontal turbulent wind speed spectrum:

$$\frac{nS_u(z,n)}{u^2} = \frac{11.4f}{(1+14.44f)^{5/3}} \quad (18)$$

Vertical turbulent wind speed spectrum:

$$\frac{nS_w(z,n)}{w^2} = \frac{5.15f}{(1+4.77f)^2} \quad (19)$$

In Eq. 18 and 19, f = nz/U, n is the gust frequency; z is the height above the arch springing and u and w are the horizontal and vertical turbulent wind speeds respectively.

CONCLUSION

Based on the measured anemometer data, the characteristics of strong winds on the site of a long-span bridge in mountainous terrian were investigated. The following conclusions were drawn:

- Measurement results showed that the wind speed varied with height, the wind speed profile of the bridge site did not fully comply with either logarithmic, or exponential, models
- Concerning mountainous terrain, the turbulence intensity was higher than that on the plains; the turbulence intensity and gust factor were significantly higher than their reference values in the Specification. The turbulence integral scale was lower than the recommended value in the Specification
- Turbulence intensity calculation results suggested that the turbulence intensity at height of 10 m above the arch springing exceeded 40%: at 90 m it was still as high as 15%. Turbulent wind posed significant problems and was a major cause of bridge buffeting

ACKNOWLEDGMENT

The authors would like to gratefully acknowledge the support of this research by National Natural Science Foundation of China (No. 50778185).

REFERENCES

Ai, X.H. and R. Xing, 2012. Advancement of research on influence factors of vortex-induced vibration of long span bridge main girder. Highway, 6: 14-15.

Andersen, O.J. and J. Lovseth, 1995. Gale force maritime wind. The Froya data base. Part 1: Sites and instrumentation. Review of the data base. J. Wind Eng. Ind. Aerodyn, 57: 97-109.

Gang, L.J., 2012. Large-span continuous steel box girder vortex-induced vibration and vibration control. Southwest Jiaotong University. http://cdmd.cnki.com.cn/Article/CDMD-10613-1012391448.htm

Ge, Y.J., Z.X. Lin, F.C. Cao, J.B. Pang and H.F. Xiang, 2002. Investigation and prevention of deck galloping oscillation with computational and experimental techniques. J. Wind Eng. Ind. Aerodynamies, 90: 2087-2098.

Gu, M., S.R. Chen and C.C. Chang, 2002. Control of wind-induced vibrations of long-span bridges by semi-active lever-type TMD. J. Wind Eng. Ind. Aerodynamics, 90: 111-126.

Lin, Z., Y.J. Ge and L.D. Zhu, 2008. Wind-excited vibration of long-span steel-lattice arch bridge under typhoon climate. Proceedings of the 4th International Conference on Advances in Wind and Structures, October 8-10, 2008, Jeju Korea, pp: 1448-1462.

Pasquill, F., 1974. Atmospheric Diffusion. Halstead Press-Wiley, New York.

Professional Standard PRC, 2004. Wind-resistent Design Specification for Highway Bridges (JTG/T D60-01-2004). China Communication Press, Beijing.

Sharma, R.N. and P.J. Richards, 1999. A re-examination of the characteristics of tropical cyclone winds. J. Wing Eng. Ind. Aerodynamics, 83: 21-33.

Shum, K.M., Y.L. Xu and W.H. Guo, 2008. Wind-induced vibration control of long span cable-stayed bridges using multiple pressurized tuned liquid column dampers. J. Wind Eng. Ind. Aerodynamics, 96: 166-192.

Simiu, E. and R.H. Scanlan, 1996. Wind Effects on Structures. John Wiley and Sons, New York.

Xian, R., H. Liao and M. Li, 2008. Calculation of Spanwise vortex-induced vibration responses of long-span bridge girder. J. Southwest Jiaotong Univ., 43: 740-744.

Xie, Y.S., A.Q. Li and H. Wang, 2009. Comparison study on experimental strong wind characteristics of Runyang suspension bridge. Acta Aerodynamica Sinica, 27: 47-51.

Zhang, L.L., Y.P. Zeng, Z.T. Yan and R. Wang, 2006. Wind tunnel test for section model of Caiyuanbai bridge over Yangtse rive. J. Chongqing Univ., 29: 134-137.

Zhang, Y., Z.T. Hu and J.X. Liu, 2008. Research on characteristics of wind field of cable-stayed bridges in the western mountainous areas. J. Wuhan Univ. Technol., 30: 154-155.

Zhang, L.L., H. Liu, Z.Y. Yang, J.M. Zhang and W.F. Tian, 2010. Full bridge buffeting response analysis of Chongqing daning river bridge. J. Exp. Fluid Mech., 5: 42-46.